V International Conference on Computational Methods for Coupled Problems in Science and Engineering
COUPLED PROBLEMS 2013
S. Idelsohn, M. Papadrakakis and B. Schrefler (Eds)

A NUMERICAL APPROACH FOR STATIC AND DYNAMIC ANALYSIS OF DEFORMABLE JOURNAL BEARINGS

DENIS BENASCIUTTI[*], MIRCEA GH. MUNTEANU[*] AND FABIO FLUMIAN[†]

[*] Università degli Studi di Udine - Dipartimento di Ing. Elettrica, Gestionale e Meccanica (DIEGM)
via delle Scienze 206, 33100 Udine, Italy
e-mail: denis.benasciutti@uniud.it, munteanu@uniud.it, www.uniud.it/

[†] Centro Ricerche Danieli - Danieli Officine Meccaniche S.p.A.
via Nazionale 41, 33042, Buttrio (UD), Italy
f.flumian@danieli.it, www.danieli.com/

Key words: Journal bearing, finite elements, elastic deformation, dynamic analysis

Abstract. This paper presents a numerical approach for the static and dynamic analysis of hydrodynamic radial journal bearings. In the first part, the effect of shaft and housing deformability on pressure distribution within oil film is investigated. An iterative algorithm that couples Reynolds equation with a finite elements (FE) structural model is solved. Viscosity-to-pressure dependency (Vogel-Barus equation) is also included. The deformed lubrication gap and the overall stress state are obtained. Numerical results are presented with reference to a typical journal bearing configuration at two different inlet oil temperatures. Obtained results show the great influence of bearing components structural deformation on oil pressure distribution, compared with results for ideally rigid components. In the second part, a numerical approach based on perturbation method is used to compute stiffness and damping matrices, which characterize the journal bearing dynamic behavior.

1 INTRODUCTION

Journal bearings are machine elements in which the applied force is entirely supported by an oil film pressure. They are used in many different engineering applications, for example as supports of rotating shafts. They are considered superior to roll-bearings because of their higher load-bearing capacity, higher operating angular speed, lower cost and easier manufacturing. Furthermore, a proper design can assure very large service lives. The early studies on the fluid-dynamic behavior of journal bearings based on the numerical solution of Reynolds equation date back to the fifties, thanks to the work of Raimondi and Boyd (R&B) [1]-[2]. They summarized results in useful dimensionless charts ready for design, which are nowadays accepted also in code standards [3].

Raimondi and Boyd analysis is based on some simplifying assumptions, as the hypothesis of constant viscosity of oil film, independency of viscosity on pressure and finally the postulation of perfectly rigid components (shaft and bushing). Such assumptions, however, can be somewhat oversimplified, considering for example that deformation of journal bearing components under imposed oil film pressure is expected to produce a change in lubrication

gap and thus a modification in the resultant pressure distribution. Moreover, also the assumption of constant viscosity and its independence from pressure should be critically reviewed, as it is experimentally known how viscosity depends, other than temperature, also on pressure, as summarized by many constitutive models [4].

It would be then of interest to investigate in more detail the correlation existing between all the above-mentioned aspects and journal bearing performance and design.

In light of the above considerations, the present paper aims to present a general numerical approach to study the static and dynamic behavior of hydrodynamic radial journal bearings, by including in the analysis the effect of the aforementioned aspects.

In the first part, attention will focus on computation of pressure distribution as a function of temperature variation within lubrication gap, viscosity-to-pressure sensitivity (according to the Vogel-Barus constitutive model [4]) and components flexibility [5]. An iterative algorithm using a finite difference scheme will be developed to solve the Reynolds equation, based on the deformed lubrication gap calculated by a coupled structural finite elements (FE) analysis. The numerical approach will compute the pressure distribution and the local stress field including shaft and bushing structural deformation. Results will clearly emphasize the strong influence of component flexibility on journal bearing performance, with a significant reduction of peak pressure caused by components deformation.

In the second part of the paper, the dynamic behavior of journal bearing will be also investigated. A numerical procedure implementing the so-called "perturbation approach" will be developed to compute the stiffness and damping matrices characterizing the dynamic behavior of hydrodynamic journal bearings. Numerical examples considering a typical journal bearing configuration will be presented.

2 JOURNAL BEARING: BASIC CONCEPTS

A typical configuration of radial journal bearing under a vertical load (see Fig. 1) consists on a shaft rotating inside a fixed support (choke), where it is usually fitted a bush. The nominal radial clearance between shaft (diameter d=2r) and choke (diameter D=2R) is c=R-r.

The steady-state response of a journal bearing is governed by the fundamental equation of lubrication theory (Reynolds equation) [6]:

$$\frac{1}{r^2}\frac{\partial}{\partial\theta}\left(\frac{h^3}{\mu}\frac{\partial p}{\partial\theta}\right)+\frac{\partial}{\partial z}\left(\frac{h^3}{\mu}\frac{\partial p}{\partial z}\right)=\frac{6U}{r}\frac{dh}{d\theta} \tag{1}$$

where $h(\theta)=c-e\cos\theta$ is the oil film thickness as a function of angular coordinate θ, symbol e is the eccentricity, $U=\omega r$ is the tangential velocity of shaft, ω is its angular velocity, $p(\theta, z)$ is the resultant oil pressure distribution, μ is the oil dynamic viscosity. The numerical solution of Reynolds equation gives the pressure distribution $p(\theta, z)$ within the lubrication gap and the system operating parameters (eccentricity, minimum lubrication gap, force resultant components, etc.).

Due to the relative velocity between shaft and support, the oil generates a pressure $p(\theta, z)$ over the attitude angle β, where p_{max} is the peak pressure that occurs at angle θ_{pmax}. The system moves in a new equilibrium configuration, where the eccentricity e characterizes the

position of shaft axis with respect to the fixed support axis, along direction defined by angle θ_{h0} (which also identifies the direction of minimum oil thickness h_0).

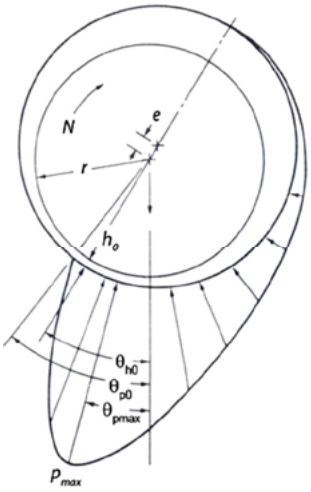

Figure 1: Sketch of a hydrodynamic journal bearing

Several design charts are available in literature [1]-[2], which provide journal bearing operation parameters as a function of Sommerfeld number $S=(r/c)^2\,(\mu N/p_m)$, defined in terms of shaft radius r and rotational speed N, while $p_m=F/(LD)$ is the average (specific) pressure defined as the ratio of the applied radial force F and the nominal projected area (L is the length of journal bearing). Such charts were determined by R&B through numerical solution of Reynolds equation under the hypothesis of constant temperature (and thus viscosity) of lubrication film and also under the assumption of perfectly rigid components (shaft and support).

An improvement of the analysis can be obtained by including in Reynolds equation a more sophisticated constitutive model for the viscosity. For example, a coupled temperature-pressure dependency can be summarized by the experimentally determined Vogel-Barus equation $\mu=\mu_0 \exp(\alpha p)$, in which μ_0 is a pressure-independent viscosity term (only function of temperature) and α is a sensitive parameter related to oil film pressure (typical values are $\alpha=0.01\div0.02$ MPa^{-1}). In accordance to this constitutive model, an increase in dynamic viscosity occurs for high pressures, with a solid-like behavior for very high pressures. This effect, well-known in elasto-hydrodynamic studies (e.g. lubricated contacts), has not been actually investigated in the field of journal bearings.

A further improvement in journal bearing analysis can be obtained by including in the solution of Reynolds equation the deformed shape of lubrication gap caused by deformation of shaft and support under imposed oil pressure $p(\theta, z)$.

This paper will present a general numerical approach to compute the pressure distribution by also including the above mentioned effects. A typical journal bearing configuration (see Table 1), operating at two different inlet oil temperatures (T_{in}=40 and 70 °C), will be investigated. A viscosity-temperature curve typical of an oil ISO VG 680 will be used in all simulations [4].

Table 1: Geometrical dimensions used in numerical simulations

d mm	D mm	L mm	F kN	N rpm	p_m MPa
500	500.5	300	3600	65	24

3 STEADY-STATE ANALYSIS

In numerical simulations two models for the journal bearing were adopted: a 2D model and a 3D one. In the first part of this paper the hypotheses used are rigid components and viscosity function of both temperature and pressure according to the Vogel-Barus model. In the second part, while shaft and support deformation will be included into the analysis, pressure effect will be considered too although it could be neglected in this case due to the drastic reduction of the maximum pressure .

3.1 Temperature and pressure effect (with rigid components)

Reynolds equation (1) is solved by using the finite difference method based on central difference scheme [7]. The unknown function in (1) is the pressure $p(\theta, z)$ that, upon integration, gives the resultant applied load F, which in fact is a given input.

It is worth noting that the problem is actually not linear for several reasons. Although the pressure $p(\theta, z)$ is the unknown function, equation (1) does not explicitly depends on load F (i.e. the resultant of pressure), but on eccentricity through the lubrication gap $h(\theta)=c-e\cos(\theta)$. Several iterations (Newton−Raphson method was used) are then required to first impose the input force F (as resultant of pressure) and to find the appropriate pressure distribution $p(\theta, z)$ that solves (1).

Table 2: Overall comparison of results from numerical simulations for rigid components, 2D model ($L/D\sim\infty$)

	Configurations		T_{in} °C	T_m °C	T_{out} °C	μ Pa·s	S -	e mm	p_{max} MPa	θ_{pmax} deg	h_0 mm	θ_{h0} deg
JB1	R&B		40	60	80	↑	↑	0.2352	87.30	15.50	0.0148	-
	T_m cost.	$\alpha=0$	↑	↑	↑	0.1678	0.00786	0.2335	82.26	15.62	0.0165	26.29
	T_m cost.	$\alpha=0.01$	↓	↓	↓	↓	↓	0.2286	83.74	15.03	0.0214	27.03
	T_{in}-T_{out} lin.	$\alpha=0$	↓	↓	↓	Not	Not	0.2392	83.17	22.82	0.0108	32.15
	T_{in}-T_{out} lin.	$\alpha=0.01$				defined	defined	0.2350	80.18	22.43	0.0150	33.76
JB2	R&B		70	80	90	↑	↑	0.2447	205.50	6.60	0.0053	-
	T_m cost.	$\alpha=0$	↑	↑	↑	0.0655	0.00298	0.2440	136.92	10.27	0.0060	16.27
	T_m cost.	$\alpha=0.01$	↓	↓	↓	↓	↓	0.2412	149.54	9.34	0.0088	16.67
	T_{in}-T_{out} lin.	$\alpha=0$	↓	↓	↓	Not	Not	0.2453	151.08	10.85	0.0047	16.18
	T_{in}-T_{out} lin.	$\alpha=0.01$				defined	defined	0.2431	173.29	9.80	0.0069	16.47

Secondly, the force-eccentricity relationship F-e is highly non-linear, especially for eccentricity values e approaching the nominal radial clearance c. Another source of non-

linearity is that negative pressure values must be set to zero during the iterative process.

Table 3: Overall comparison of results from numerical simulations for rigid components, 3D model (L/D=0.6)

Configurations		T_{in} °C	T_m °C	T_{out} °C	μ Pa·s	S -	e mm	p_{max} MPa	θ_{pmax} deg	h_0 mm	θ_{h0} deg
JB1	R&B	40	60	80	↑	↑	0.2405	158.00	6.00	0.0095	-
	T_m cost. $\alpha=0$				0.1678	0.00786	0.2397	152.43	6.15	0.0103	16.34
	T_m cost. $\alpha=0.01$				↓	↓	0.2357	219.08	7.50	0.0143	16.59
	T_{in}-T_{out} lin. $\alpha=0$	↓	↓	↓	Not	Not	0.2442	179.06	8.28	0.0058	14.34
	T_{in}-T_{out} lin. $\alpha=0.01$				defined	defined	0.2411	285.85	6.97	0.0089	14.67
JB2	R&B	70	80	90	↑	↑	0.2456	269.39	3.10	0.0044	-
	T_m cost. $\alpha=0$				0.0655	0.00298	0.2452	203.07	5.95	0.0048	11.66
	T_m cost. $\alpha=0.01$				↓	↓	0.2424	407.09	5.25	0.0076	11.82
	T_{in}-T_{out} lin. $\alpha=0$	↓	↓	↓	Not	Not	0.2464	221.00	6.11	0.0036	10.82
	T_{in}-T_{out} lin. $\alpha=0.01$				defined	defined	0.2438	674.38	4.56	0.0062	10.97

To evaluate the effect of temperature on viscosity, and consequently on pressure distribution, the journal bearing configuration in Table 2 (2D model) and Table 3 (3D model) was studied at two operating conditions (JB1, JB2) characterized by two different inlet temperatures (T_{in}=40, 70°C). Two hypotheses are then adopted to compute the pressure-independent viscosity term μ_0 as a function of oil temperature: in the first, using an average constant oil temperature T_m resulting by a thermal balance inside the oil film (as in R&B approach), in the second using, as a first approximation, a linear temperature variation from inlet value T_{in} to the outlet value T_{out} (that has been calculated by previous thermal balance). Note that in both cases the same average oil film temperature T_m is obtained.

For both temperature distributions within lubrication gap (constant T_m, linear T_{in}-T_{out}), the Vogel-Barus equation has been implemented with two different cases (α=0 and α=0.01).

Table 2 shows an overall comparison of obtained results for the 2D model and Table 3 the comparison for the 3D model. Figures 2 and 3 compare the pressure distribution under an imposed vertical load, with a linear temperature variation within oil film and assuming different pressure sensitivity values for viscosity. As expected with 3D model it results larger values for maximum pressure because the 2D model assumes a constant distribution along shaft axis.

The effect of temperature variation of oil film is first analyzed. Referring to JB1 configuration in Table 2, a negligible difference is observed between the case of constant and linearly varying temperature, for both α=0 and α=0.01 values. Instead, larger differences (with a 10-12% increase of p_{max} value) are observed for JB2 configuration, considering both α=0 and α=0.01 values. On the contrary, for 3D model the value of maximum pressure, much larger with respect of 2D case, strongly depends on α sensitivity factor. Also p_{max} depends on temperature variation law.

This emphasizes how the variation of oil film temperature could have some effect on

pressure distribution, especially for high temperature values. Considering the viscosity-temperature strong correlation, this seems to confirm that pressure distribution is more sensitive to a change of viscosity values within lubrication gap. Constant viscosity assumption used in R&B calculations (no temperature and no pressure influence) seems too simplified.

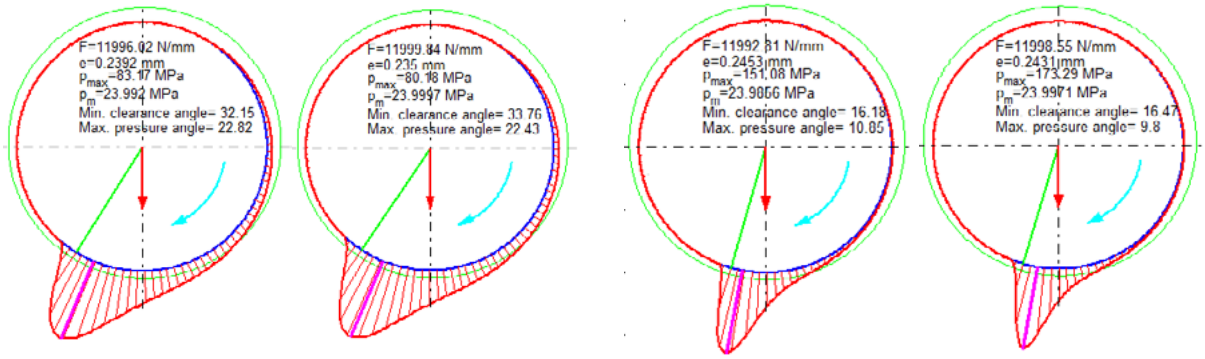

α=0, p_{max}=83.17 MPa α=0.01, p_{max}= 80.18 MPa α=0, p_{max}= 151.08 MPa α=0.01, p_{max}= 173.29 MPa

a) JB1 configuration (linear temperature variation, T_{in}= 40°C – T_{out}=80 °C)

b) JB2 configuration (linear temperature variation, T_{in}= 70°C – T_{out}=90 °C)

Figure 2: Results for JB1 and JB2 configurations, 2D model

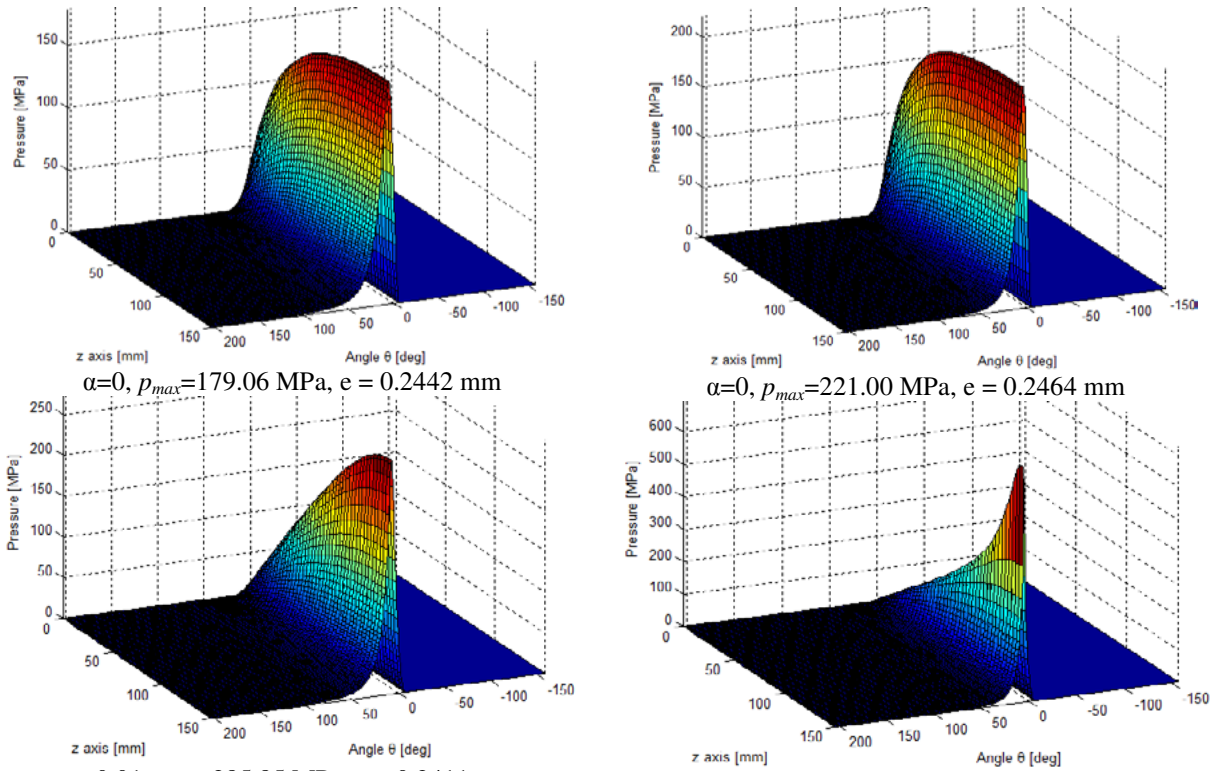

α=0, p_{max}=179.06 MPa, e = 0.2442 mm α=0, p_{max}=221.00 MPa, e = 0.2464 mm

α=0.01, p_{max}=285.85 MPa, e = 0.2411 mm α=0.01, p_{max}=674.38 MPa, e = 0.2438 mm

a) JB1 configuration (linear temperature variation, T_{in}= 40°C – T_{out}=80 °C)

b) JB2 configuration (linear temperature variation, T_{in}= 70°C – T_{out}=90 °C)

Figure 3: Results for JB1 and JB2 configurations, 3D model

On the other hand, in the case of rigid components (shaft and bushing), the 2D model to solve Reynolds equation (1) is not suitable as pressure distribution is very different from 3D model, see figures 2 and 3.

Numerical solutions for constant T_m and α=0 were also compared with results given by R&B charts, showing a good agreement only for JB1 configuration, while some difference characterizes JB2 configuration. The observed discrepancy can be attributed to the very low Sommerfeld number (S=0.00298) characterizing JB2 configuration, which makes difficult using R&B design charts and thus can be source of interpolation errors.

A non-zero viscosity-to-pressure sensitivity (α=0.01) determines an important variation in the overall pressure distribution (change of attitude angle β) and in its maximum value p_{max}, depending on the general pressure levels attained. In the case of 2D model with T_{in}-T_{out} linear temperature variation, for peak pressures p_{max}<100 MPa (2D model, case JB1), the pressure effect is actually negligible, as shown in Fig. 2a, with only a small decrease of the maximum pressure of about 3.5%. For larger pressure levels (case JB2), an increment of p_{max} of about 12% is observed, see Fig. 2b. The minimum oil thickness increment (h_0=c-e) produced by the pressure effect is relevant in both cases, with a variation respectively of 28% and 32%.

For the 3D model the maximum pressure are much higher and the effect of α is extremely important. The minimum film oil thickness has the same tendency as in the previous case but the values are larger: 37% and 42% respectively.

The obtained results can be summarized by saying that, if the influence of pressure on viscosity is taken into consideration, when α increases the peak pressure p_{max} increases, while the eccentricity e decreases. The conclusion of detailed study shows that the pressure-to-viscosity effect is smaller compared to temperature influence if the maximum pressure is smaller than 90…100 MPa and in this case could be neglected.

3.2 Effect of component deformation (T linear)

In the second part of this work, the pressure distribution will be calculated by considering the real geometry of lubrication gap resulting from component deformation. Pressure values calculated by solving the Reynolds equation (1) are used, as input in a FE model, to compute the geometry of lubrication gap after deformation, which is next used to solve again equation (1) with an iterative analysis scheme. Details on the numerical algorithm can be found in [7].

A fluid-structural coupled numerical procedure was developed in Matlab environment. The first analysis step is the calculation of pressure distribution $p(\theta, z)$ and eccentricity e for the case of not deformable components, by solving Reynolds equation (1). The obtained pressure distribution is next applied as input mechanical load in a plane structural FE model, which gives the relative radial displacements between shaft and support after deformation, and the resulting gap deformation $g(\theta, z)$. A new oil film geometry $h'(\theta, z)=c-e\cos(\theta)+g(\theta, z)$ that incorporates mechanical deformation (thus it differs from the case of perfectly rigid components) can be thus calculated. At second iteration step this updated gap geometry $h'(\theta)$ is entered in (1) to get a new pressure distribution $p'(\theta, z)$ that balances the input force F. This iterative procedure is repeated until convergence is achieved with respect to an imposed threshold tolerance on the maximum pressure [7].

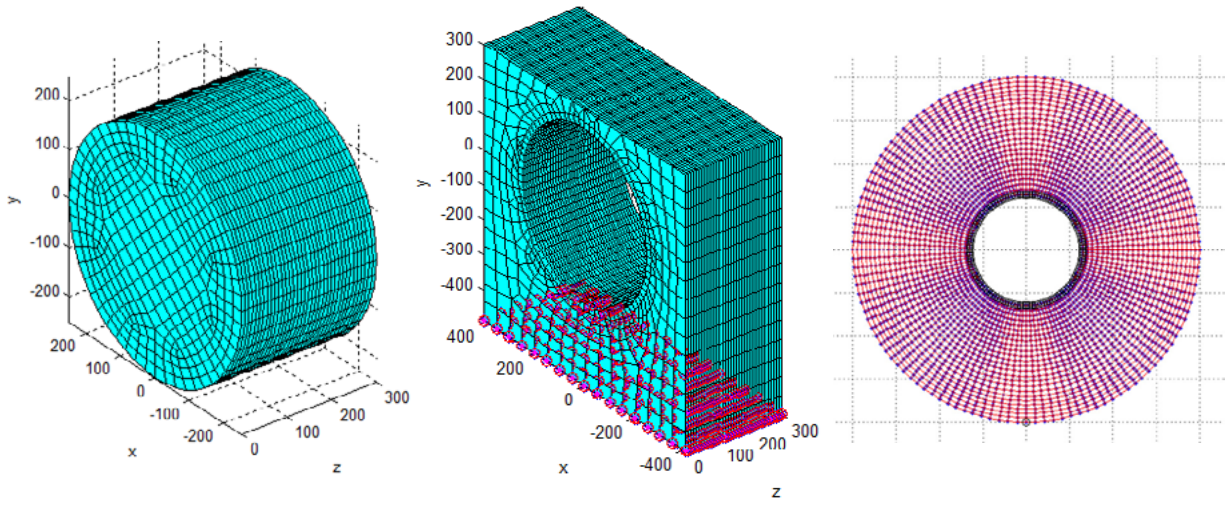

a) 3D model: 13616 nodes, 12276 8-node finite elements

b) 3D model : 16613 nodes, 13644 8-node finite elements

c) 2D model for shaft

Figure 4: Finite element model of shaft and support

The 3D FE models of both shaft and support used in the analysis are shown in figures 4a and 4b. The shaft and the support are modeled by a *mesh* with 8-node brick isoparametric finite elements. The 2D model uses 4-node plane isoparametric finite element. The support is fixed on the lower surface, while the shaft is clamped on one end (z=300 mm, Fig. 4a).

Shaft and support are loaded by the same oil pressure distribution $p(\theta, z)$ applied on the outer and inner surfaces, respectively. Analysis assumes small displacements. In the case of 2D model a plane strain condition was considered. Material has linear elastic behavior, with properties typical of a structural steel.

It is worth noting that the use of a plane FE model for the structural analysis of a journal bearing requires a special attention in modeling mechanical constraints. In fact, in a real journal bearing the applied load F and the resulting pressure distribution are actually applied along different longitudinal locations along the shaft axis. Instead, in the plane FE model here adopted the external load F that balances the oil pressure is replaced by an appropriate constrain on shaft geometry. For this purpose, the shaft has been modeled with a central hole and all nodes on the inner circumference have imposed zero radial displacements, Fig 4c; the support, instead, has all the external edges constrained. This modeling strategy, however, affects the shaft structural stiffness: a large inner radius determines an anomalous increment of shaft stiffness, while a very small inner hole gives rise to very large deformations and abnormally high reaction forces at constrained nodes. A proper sensitivity analysis has been preliminary carried out, in order to find the optimal radius of inner hole.

The coupled numerical approach was applied to study the JB1 configuration (with α=0.01 and linear temperature variation in T_{in}=40°C–T_{out}=80°C). Fig. 5 shows the result for the case of deformable components, 3D model. The comparison with the case of rigid components in Fig. 3a clearly emphasizes how component deformation determines a reduction to about 20% (285.85 MPa to 56.04 MPa) of the maximum peak pressure in the median plane of the shaft (Fig. 5b) and, accordingly, an increase in the attitude angle β (under the same applied resultant

force F). The pressure profile, more uniform than the case of rigid components (R&B solution), seems to support the idea of using the average pressure p_m as a structural design parameter, as suggested in some design codes [3].

The absolute maximum of the pressure is around 65…85 MPa add it is reached at the two ends of the shaft. This value depends on the local mesh fineness and this aspect will be discussed in a future paper. The 2D model gives a value of maximum pressure (considered valid in the median shaft section) of 49.98 MPa, closed enough to 3D model.

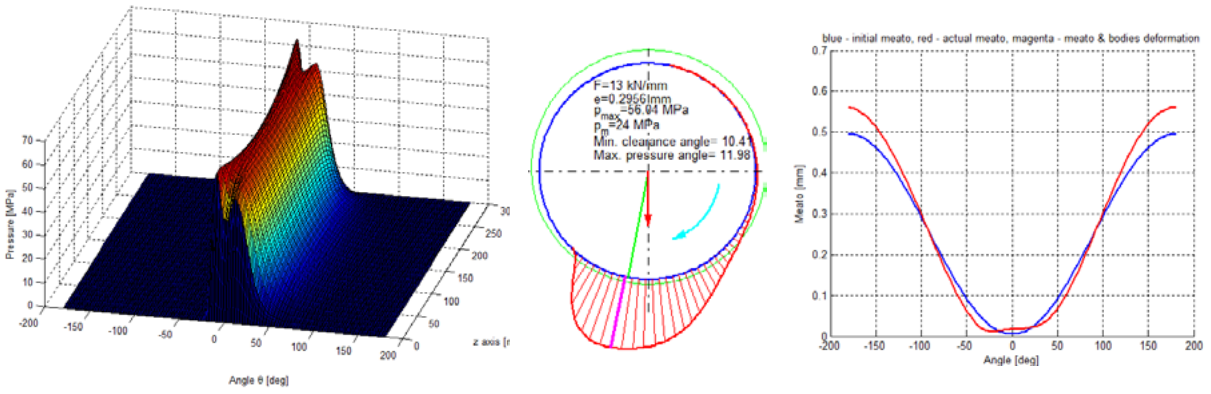

a) Presure distribution

b) pressure distribution in the middle section

c) Lubrication gap for rigid (blue) and deformable components (red)

Figure 5: Pressure distribution, JB1 configuration (α=0, T= 40° - 80 °C), deformable components, 3D model

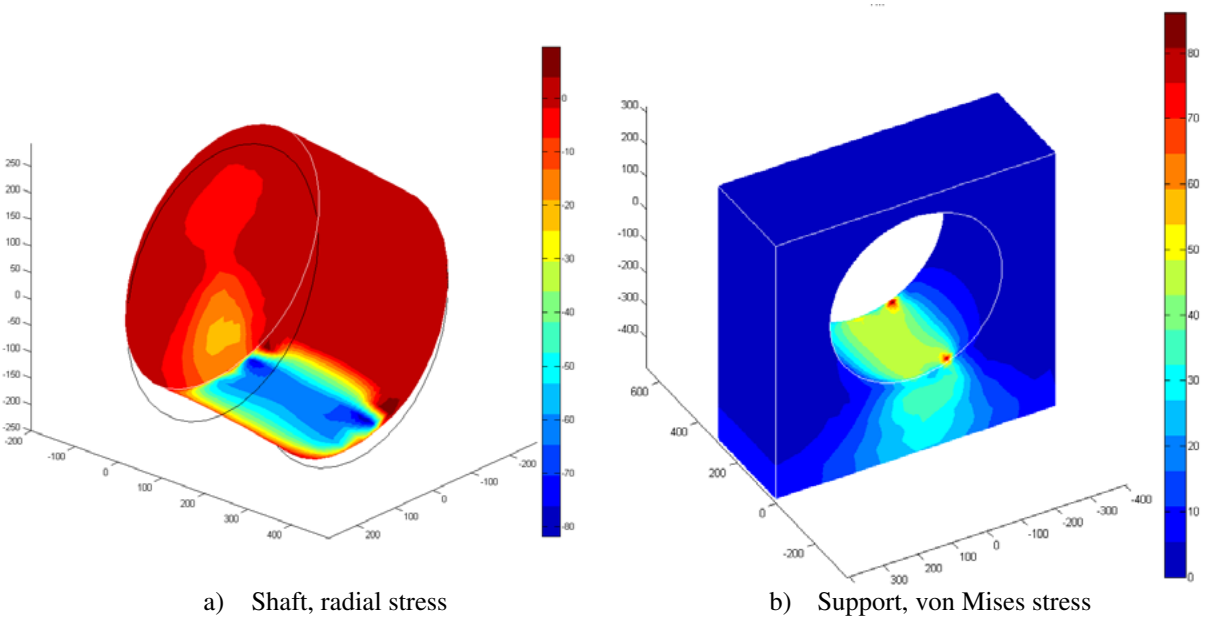

a) Shaft, radial stress

b) Support, von Mises stress

Figure 6: Stress distribution (MPa units)

Fig. 5c also compares the geometry of lubrication gap for the case of deformable and rigid components (angles are referred to the position of minimum oil gap θ_{h0}). It is observed that

for deformable components the gap is not symmetric and that eccentricity can assume values greater than the nominal clearance, as deformation can increase the gap between shaft and support.

For what concerns the calculated mechanical stresses, Fig. 6 shows stress distribution in the shaft (radial stress) and in the support (von Mises stress). Compared to the case of perfectly rigid components, this explains the relatively small values of von Mises stress calculated in the support, which is actually comparable with static strength of materials usually employed in the bush (for instance, white metal generally used as internal coating has a yield stress of about 50 MPa [5]).

4 DYNAMIC ANALYSIS

The dynamic behavior of rotating shaft supported by journal bearings is strongly influenced by the hydrodynamic forces produced in lubricant film that oppose to shaft movement. Determination of rotor dynamics then requires full characterization of the dynamic response of bearing lubricant film, which is a non-linear function of position and velocity of journal center.

In the dynamic analysis of a rotor-bearing configuration, a simple spring-dashpot model is usually adopted to account for journal bearing contribution [6]. With small displacements increments (δx, δy) and small velocities increments ($\delta\dot{x}$, $\delta\dot{y}$) in the vicinity of the journal bearing static equilibrium position, a linearized relationship, between the incremental oil-film forces δF_i and journal displacements and velocities increments that cause them, can be written as [6]:

$$\begin{pmatrix} \delta F_x \\ \delta F_y \end{pmatrix} = -\begin{bmatrix} k_{xx} & k_{xy} \\ k_{yx} & k_{yy} \end{bmatrix}\begin{pmatrix} \delta x \\ \delta y \end{pmatrix} - \begin{bmatrix} c_{xx} & c_{xy} \\ c_{yx} & c_{yy} \end{bmatrix}\begin{pmatrix} \delta\dot{x} \\ \delta\dot{y} \end{pmatrix} \tag{2}$$

where $k_{ij} = (\delta F_i / \delta x_j)$ and $c_{ij} = (\delta F_i / \delta\dot{x}_j)$ are the linear stiffness and damping coefficients, respectively.

A classical "perturbation method" is followed to compute the increase in oil film forces resulting from a departure (perturbation) from the static equilibrium position. A journal bearing configuration, characterized by given displacement (u, v) and velocities $(\dot{u}, \dot{v})$ of journal centre, is first assigned. The reference pressure distribution $p(\theta, z)$ and oil film forces F_x and F_y are then calculated by Eq. (3), the Reynolds equation in dynamic regime:

$$\mu\frac{h^3}{r^2}\frac{\partial}{\partial\theta}\left(\frac{1}{\mu}\frac{\partial p}{\partial\theta}\right) + \frac{3h^2}{r^2}\frac{\partial h}{\partial\theta}\frac{\partial p}{\partial\theta} = \frac{6U\mu}{r}\frac{\partial h}{\partial\theta} + 12\frac{\partial h}{\partial t} \tag{3}$$

which explicitly depends also on the time derivative of lubrication gap $\dot{h}(\theta) = -\dot{u}\cos\theta - \dot{v}\sin\theta$. Independent displacement and velocity perturbations are next applied and the corresponding force increments calculated. Solution of (3) gives the increased pressure distribution (say $p+\delta p$), and therefore the increased resultant of oil film forces $F_x+\delta F_x$ and $F_y+\delta F_y$, with respect to the reference equilibrium position, for shaft displacement and velocity increments $(\delta x, \delta y, \delta\dot{x}, \delta\dot{y})$. Thus stiffness and damping coefficients can be thus

determined, as for example:

$$[k] \approx \begin{bmatrix} \frac{\delta F_x}{\delta u} & \frac{\delta F_x}{\delta v} \\ \frac{\delta F_y}{\delta u} & \frac{\delta F_y}{\delta v} \end{bmatrix} \tag{4}$$

To include also the contribution of the structure deformation into stiffness and damping matrices, in the above expression the displacement increments are substituted by δu_o and dv_o, total displacement increments of the bearing center. Absolute displacements u_o and v_o of the bearing center and their increments δu_o and dv_o are found as explained in section 3.2. A similar approach is used to determine damping matrix.

Stiffness [k] and damping [c] matrices characterize the dynamic behavior of journal bearing and they enter into the dynamic equilibrium equations of the shaft. It is worth noting that, due to the non-linear nature of the Reynolds equation (3), both matrices explicitly depend on the assigned journal bearing displacement (u, v) and velocities $(\dot{u}, \dot{v})$, that is they have to be interpreted as tangent matrices. Therefore, a transient dynamic analysis of a rotor supported by journal bearings is non-linear and [k], [c] matrices must be calculated at every time integration step. In addition, [k] and [c] are in general not symmetric.

A numerical algorithm has been specifically developed to compute stiffness and damping matrices by the perturbation method previously described. The procedure has been applied to characterize different journal bearing configurations.

An example of calculated pressure distribution for JB1 configuration for two different velocities, $\dot{v} = 0$ and $\dot{v} = 0.5$ mm/s , is shown in Fig. 7 (2D model). The calculated stiffness and damping coefficients are reported in Fig. 8 and Fig. 9: a high non-linear dependence on the eccentricity e is observed.

5 CONCLUSIONS

The present papers developed a numerical procedure for the steady state and dynamic analysis of hydrodynamic radial journal bearing. Influence of temperature and pressure on viscosity and thus on resultant pressure distribution were studied. A mechanical plane finite element model, coupled with solution of Reynolds equation, was also developed to study journal bearing structural behavior and its influence on pressure distribution. Finally, a perturbation approach was implemented to evaluate stiffness and damping coefficients.

The main findings of the work can be summarized as follows:

- temperature increase was shown to give a decrease of attitude angle β and an increase in pressure peak;
- an increase of viscosity-to-pressure sensitivity (α value) gives a general increase of peak pressure for pressure peaks greater than about 90…100 MPa;
- component deformation gives a more uniform pressure distribution, with a considerable reducing of the peak pressure compared to the case of ideally rigid components;
- stiffness and damping coefficient were calculated and a high non-linear trend with journal bearing eccentricity e was observed.

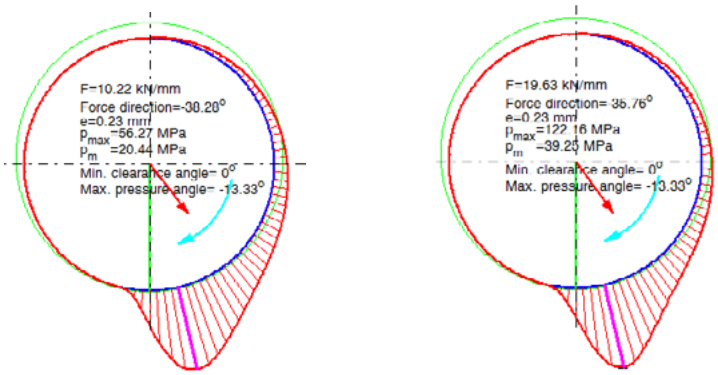

Figure 7: Pressure distribution calculated for u=0, $\dot{u}=0$, v=0.23 mm and $\dot{v}=0$ (left) and $\dot{v}=0.5$ mm/s (right)

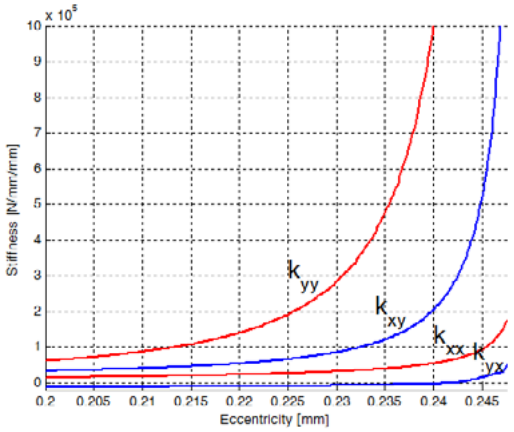

Figure 8: Stiffness coefficients [N/mm/mm], JB1,versus eccentricity (for u=0, $\dot{u}=0$, $\dot{v}=0$)

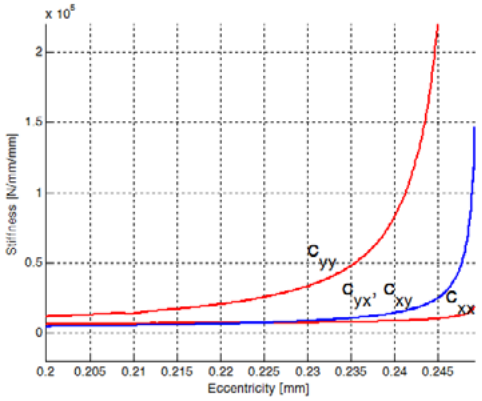

Figure 9: Damping coefficients [Ns/mm/mm], JB1, versus eccentricity (for u=0, $\dot{u}=0$, $\dot{v}=0$)

REFERENCES

[1] Boyd, J., Raimondi, A.A. Applying bearing theory to the analysis and design of journal bearings, *J. Appl. Mech.*, *Trans. ASME* (1951) **73**: 298-309 (Part I), 310-316 (Part II).

[2] Raimondi, A.A., Boyd, J. A solution for the finite journal bearing and its application to the analysis and design, *Trans. ASLE*(1958) **1:**159-174 (Part I), 175-193 (Part II), 194-209 (Part III).

[3] DIN 31652, Hydrodynamic plain journal bearings designed for operation under steady-state conditions, Part 1-3 (1983).

[4] Stachowiak, G.W., Batchelor, A.W. *Engineering Tribology* (Third Edition), Elsevier Butterworth-Heinemann, Burlington (2005).

[5] ASM Handbook, *Properties and selection: nonferrous alloys and special-purpose materials*. ASM International, Vol. 2, (1990).

[6] Szeri, A.Z. *Fluid film lubrication* Cambridge University Press, 2nd ed. (2011).

[7] Benasciutti, D., Gallina, M., Munteanu, M.Gh. and Flumian, F. A numerical approach for the analysis of deformable journal bearings, Frattura e Integrità strutturale (2012) **21**: 37-45.

[8] Frene, J., Nicolas, D., Berthe, B. and Godet, M. *Hydrodynamic lubrication*, Elsevier (1990).